ORIGINAL PAPER   **Open Access**

A novel to perform a thermoelastic analysis using digital image correlation and the boundary element method

Check for updates

Matheus B. A. M. Oberg, Daniel F. de Oliveira, Jhon N. V. Goulart and Carla T. M. Anflor[*]

Abstract

This work aims for a novel thermoelastic analysis methodology based on experimental steady-state temperature data and numerical displacement evaluation. The temperature data was acquired using thermal imaging and used as the input for a boundary element method (BEM) routine to evaluate its consequent thermoelastic displacement. The thermoelastic contribution to the resultant displacement arises in the BEM formulation as a domain integral, which compromises the main benefits of the BEM. To avoid the necessity of domain discretization, the radial integration method (RIM) was applied to convert the thermoelastic domain integral into an equivalent boundary integral. Due to its mathematical development, the resultant formulation from RIM requires the temperature difference to be input as a function. The efficacy of the proposed methodology was verified based on experimental displacement fields obtained via digital image correlation (DIC) analysis. For this purpose, a CNC (computer numerical control) marker was developed to print the speckle pattern instead of preparing the specimen by using manual spray paint or using commercially available pre-painted adhesives. The good agreement observed in the comparison between the numerical and experimental displacements indicates the viability of the proposed methodology.

Keywords: Boundary element method, Radial integration method, Thermoelasticity, Digital image correlation, Thermal images

Introduction

Machines and structures under the effect of thermal loadings have always been of great importance for the development of our global society. This kind of machinery and structures still assumes fundamental roles in societies, such as in aerospace transportation, in the form of combustion engines, energy generation, heated pipelines and pressure vessels, among others. In the face of the constant demand for safer and more efficient designs, several different numerical simulation methods have been developed to provide accurate solutions for a growing variety of problems. Among the available numerical methods, the boundary element method (BEM) has been experiencing an increase in popularity over the last decades. This is driven by a continuous development

effort in expanding its applications and computational viability.

Due to its significance to engineering, the boundary integral formulation for thermoelastic problems, detailed in Sládek and Sládek (1983, 1984), was probably one of the first BEM formulations to be studied. During its mathematical development, the thermal component of displacement arises naturally as a domain integral. The presence of a domain term compromises the BEM's main characteristic, which is the solution of problems using exclusively boundary discretization. Since the consolidation of BEM as a numerical tool, many different techniques have been elaborated to overcome this issue, which is common in problems involving body forces. In an early effort, Cruse (1975) presented a solution for centrifugal force using divergence theorem. Later, Danson (1981) proposed a different approach based on the Galerkin vector and the Gauss-Green theorem concerning gravitational loadings and centrifugal forces. The

* Correspondence: anflor@unb.br
Group of Experimental and Computational Mechanics, University of Brasilia, Gama, Brasilia, Brazil

search for a more general method, able to deal with a wider variety of problems, lead to the development of the dual reciprocity method (DRM), presented in Nardini and Brebbia (1983) and detailed in Partridge, Brebbia, and Wrobel (1992). This method relies on using radial base functions (RBF) to approximate the effects of body forces and is, perhaps, the most used method currently. Even though it has high acceptance, the RBF used for the approximations are not unique. Hence, to assure the quality of the provided results, the DRM also demands an assessment analysis of the applied RBF for every specific problem. Aiming to solve problems governed by the Helmholtz and Poisson equations, Nowak and Brebbia (1989) introduced the multiple reciprocity method (MRM). This method was later extended for the solution of Navier equations for elasticity in Neves and Brebbia (1991) and to solve arbitrary body force problems in Ochiai and Kobayashi (1999), as stated in Gao (2003).

As an alternative method, Gao (2003) presented a purely mathematical approach, the radial integration method (RIM), capable of converting domain integrals to equivalents over the boundary. Due to its exclusively mathematical procedure, it can provide precise conversions for domain integrals of any kind. Unlike the MRD, this method requires the acting body force to be input as a function instead of individual values. Gao (2003) presents a thermoelastic BEM formulation using RIM to convert the term responsible for the thermoelastic contribution to an equivalent boundary integral. Given constant material properties, the resultant boundary integral ends up as a function of the temperature distribution over the domain. In common engineering scenarios, temperature readings are often obtained as a set of punctual readings. In this sense, the application of the formulation presented in Gao (2003) requires, beforehand, the use of some sort of fitting tool to approximate the entire data set to a continuous function, which may introduce a source of error to the problem.

In real engineering situations, it is often possible to assess the acting boundary conditions over a domain using reverse engineering principles. In the case of thermoelastic problems, the acting temperature field can be obtained using a thermal imaging procedure, such as the one presented in Dondero et al. (2011). This information can be used as an input for numerical analysis to evaluate the displacement field caused by the acting temperature field.

At the same time, the resultant displacement field can also be experimentally evaluated using a digital image correlation (DIC) analysis. This optical metrology technique, detailed in Pan, et al. (2009), relies on the comparison between digital images of the target surface in a non-loaded situation and after the application of a deformational loading. To calculate the full-field displacement solution, this method requires the surface under investigation to have a random speckle pattern marked over it. This pattern is mapped by the DIC system and used as a reference to evaluate the resultant displacement field. Thus, as stated in several works, such as Barranger et al. (2010), Lecompte et al. (2006), Lecompte, Sol, and Vantomme (2006), and Pan et al. (2009), the quality of the marked pattern has considerable influence on the quality of the obtained results. Considering the lack of control in typical spray-painting techniques for pattern generation, as stated in Crammond, Boyd, and Dulieu-Barton (2013), Mazzoleni et al. (2015) proposed a thermo-mechanical toner device to reproduce numerical generated speckle patterns. Unlike the more traditionally generated speckle patterns, numerically generated patterns can consistently reproduce better speckle size and distribution parameters, like the ones presented in Lecompte et al. (2006). However, while the non-uniformity of the surface is advantageous to the DIC analysis, it also has negative effects on the quality and the precision of the thermal images data. This issue is evinced in Bodelot et al. (2009) and Silva and Ravichandran (2011), in which the DIC and thermal images are used together on the same surface to assess thermoelastic effects and demanded the use of special coatings. Efforts to increase the accuracy of DIC data acquisition is a still current subject. In this sense, the efforts are concerned with controlling the generation of the speckle patterns that generally are made manually by spraying the paint on the specimen. It is well known that generating an optimal design of speckle patterns plays an important role in the accuracy for obtaining the strain displacement. Recently, a novel method using an atomization system to repeatedly generate speckle patterns was introduced by Zhang et al. (2018) and an innovative approach to DIC using a QR (quick response) code-based random speckle pattern was successfully employed by Krishna et al. (2019) for the structural health monitoring of beams. Problems related to thermoelasticity are still a current theme in several areas of engineering. Optical methods are one of the best options for measuring the displacement and temperature field and are widely used for monitoring structures such as vessels (Paiva et al., 2018), brakes (Serrano-Munoz et al., 2019) or even welding processes (Chen, Sun, Dulieu-Barton, Li, & Wang, 2018), among many other applications. As previously mentioned, new methodologies for speckle pattern generation used for DIC coupled with heat transfer measurement still need attention.

This work presents a methodology for thermoelastic analysis based on experimental temperature data acquisition and numerical displacement evaluation via BEM. The temperature field acquisition was executed via

thermal imaging and used as an input, together with the acting mechanical boundary conditions, in a thermoelastic BEM routine based on the RIM formulation presented in Gao (2003). The combination of both techniques allows for the numerical evaluation of the displacement field caused by the acting temperature field. A polynomial fitting tool was used to approximate the array of punctual temperature data as a function of its coordinates. This work also presents an experimental procedure based on simultaneous DIC and thermal image analyses to verify the proposed methodology and provide reference data for posterior error analyses. It relies on the simultaneous acquisition, via thermal images, of the acting temperature on a subject submitted to a controlled heating and its consequent displacement field using a bidimensional DIC analysis. Inspired by Mazzoleni et al. (2015), a prototype CNC (computer numerical control) marker device was developed to ensure the controlled marking of computer-generated speckle patterns over the studied surfaces. It is worth mentioning that despite several works regarding thermoelastic problems, few of them consider the numerical modelling and experimental procedure simultaneously. A novel in detail experimental procedure and the development of a CNC marker also contributes to enhancing the generation of the speckle patterns required for DIC acquisition. As far as the authors are aware, the present methodology involving CNC marker development, BEM and RIM modelling, and the use of DIC techniques is novel.

This paper is organized as follows. In the "Methods" section, the BEM for thermoelasticity is presented, as well as the procedure for transforming the domain integrals for displacement into equivalent boundary integrals using RIM. The DIC analysis is presented in the "Digital image correlation analysis" section. The experimental design and setup and the verification of the proposed methodology are presented in the "Results and discussion" section. Finally, the conclusions are presented and discussed in the "Conclusions" section.

Methods

In this work, a simple rectangular aluminium plate was heated by a cartridge resistance, generating a temperature field distribution causing a strain field due to the expansion thermal effect. Temperature-elasticity fields occurring simultaneously on a body give rise to thermoelastic problems. This class of problem can be modelled by several numerical methods. Specifically, for this case, BEM coupled to the RIM technique was employed to numerically evaluate the temperature and strain fields. RIM is a purely mathematical approach to convert domain integrals into boundary equivalents, allowing solving problems with domain thermal load, and thus, preserving the main feature of the BEM. The

body forces herein are represented by the temperature field due to the cartridge resistance heating. The temperature field was acquired on one of the plate's sides by means of a thermal camera. An experimental procedure using the DIC methodology was performed on the opposite face of the plate. Both experimental and numerical data are used posteriori to support the numerical results. It is well known that the accuracy of the displacement field by DIC depends on the quality of the speckle pattern generated. A CNC marker was fully developed and the quality of the generated speckle pattern was investigated. In the case of the present work, the proposed methodology could be applied to thermoelastic problems involving complex geometries, such as engines. Also, preserving the advantages of the boundary-only method, provided by BEM and RIM, will make it easy to employ with CAD platforms since only the surface information is needed for modelling.

The boundary element method for thermoelasticity

The steady-state thermoelasticity formulation can be used to describe a broad range of engineering problems. In this sense, its boundary integral formulation has been featured in several works and can be found in detail in many books, such as Aliabadi (2002), Banerjee and Butterfield (1981) and Katsikadelis (2002). One of the main features of BEM is to provide a complete problem solution in terms of boundary values only, making it a low-cost computational method and suitable to be straightforwardly used with CAD platforms. For a thermoelastic analysis, the body force is represented by the generated temperature field that causes strains due to the expansion thermal effect. Thus, RIM is used to reduce the domain integral to a boundary integral allowing the use of BEM with its features preserved.

Considering a homogeneous body, illustrated in Fig. 1, with a linear isotropic constitutive relationship, the steady-state thermoelasticity is described by the equilibrium and Laplace equations,
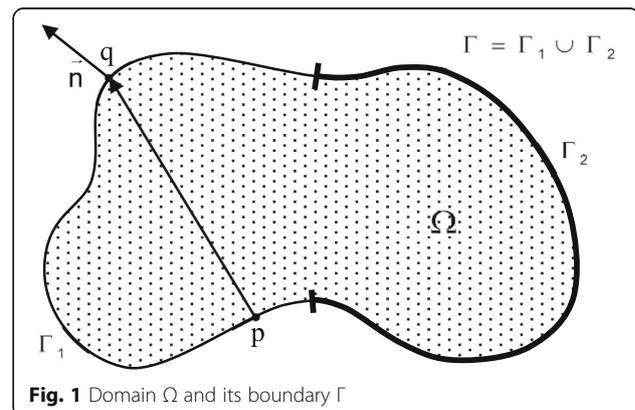

Fig. 1 Domain Ω and its boundary Γ

$$\sigma_{ij,j}(x) + b_i(x) = 0, \quad \forall x \in \Omega \tag{1}$$

$$\nabla^2 \theta(x) = 0, \forall x \in \Omega \tag{2}$$

where $\sigma_{ij,\,j}$ are derivatives of the stress components, b_i are the body forces and θ corresponds to the temperature field acting over the domain (Ω).

Following the development presented in Gao (2003), a body submitted to a distributed thermal load experiences a purely volumetric expansion in addition to the effects caused by typical mechanical loadings. Therefore, for these cases, the relationship between the total strain (ε_{ij}), and the components of the stress tensor (σ_{ij}) are given by,

$$\varepsilon_{ij} = \frac{1}{2G}\left\{\sigma_{ij} - \frac{\nu}{1+\nu}\delta_{ij}\sigma_{kk}\right\} + \delta_{ij}k\theta \tag{3}$$

where G is the material's shear modulus, ν is Poisson's ratio, δ_{ij} is the Kronecker delta and k is the material's coefficient of thermal expansion. The indexes i, j, k follow the rules of suffix notation. The first term on the RHS of Eq. (3) represents the strain produced by the actual stress while the second represents the thermal expansion effect. From Eq. (3), (σ_{ij}) can be written as,

$$\sigma_{ij} = 2G\left\{\varepsilon_{ij} + \frac{\nu\delta_{ij}\varepsilon_{kk}}{1-2\nu}\right\} - \delta_{ij}\tilde{k}\theta \tag{4}$$

$$\tilde{k} = \frac{2G(1+\nu)k}{1-2\nu} \tag{5}$$

Equation 4 resembles the equilibrium equation typically presented in BEM formulation for elastostatics with the thermal expansion term assuming the role of the body force. Thus, applying Betti's reciprocal theorem as shown in Aliabadi (2002) to Eq. (4) leads to,

$$\int_\Omega \left(\sigma_{ij}\varepsilon_{ij}^* + \tilde{k}\theta\varepsilon_{kk}^*\right) d\Omega$$
$$= \int_\Omega \left(\sigma_{ij}^*\varepsilon_{ij} + \tilde{k}\theta^*\varepsilon_{kk}\right) d\Omega \tag{6}$$

$$\int_\Omega u_k \sigma_{kj,j}^* \, d\Gamma + \int_\Omega \tilde{k}\theta\varepsilon_{kk}^*$$
$$= -\int_\Gamma t_k u_k^* \, d\Gamma + \int_\Gamma u_k t_k^* \, d\Gamma \tag{7}$$

where u_k and t_k are the displacements and tractions, respectively, and the presence of the ' * ' symbol represents fundamental solutions of the boundary integral equations.

From the Dirac delta function properties and the considerations to extend the formulation to the boundary, presented in Brebbia and Dominguez (1996), Eq. (7) becomes,

$$c_{ij}u_j + \int_\Gamma \left(T_{ij}u_j - U_{ij}t_j\right) d\Gamma = \int_\Omega U_{ij,j}\tilde{k}\,\theta\,d\Omega \tag{8}$$

where $c_{ij} = 0.5\,\delta_{ij}$ for collocation points located over smooth boundaries, $c_{ij} = \delta_{ij}$ when the collocation points are inside the domain and $c_{ij} = 0$ for collocation points outside the domain. The terms U_{ij} and T_{ij} are, respectively, the Kelvin fundamental solutions for two-dimensional displacement and traction, described by the following equations,

$$U_{ij} = \frac{1}{8\pi(1-\nu)G}\left[-(3-4\nu)\,\delta_{ij}\,\ln(r) + r_{,i}r_{,j}\right] \tag{9}$$

$$T_{ij} = \frac{-1}{4\pi\,r\,(1-\nu)}\left\{\frac{\partial r}{\partial n}\left[(1-2\nu)\delta_{ij} + 2r_{,i}r_{,j}\right] - (1-2\nu)\left(r_{,i}n_j - r_{,j}n_i\right)\right\} \tag{10}$$

where r represents the distance between the field and source point and n is the unit normal vector outward.

The differentiation between Eq. (9) substituted into the domain integral term obtained in Eq. (8) results in,

$$\int_\Omega U_{ij,j}\tilde{k}\,\theta\,d\Omega = \int_\Omega \frac{-(1+\nu)k}{2\pi(1-\nu)r}\,r_{,i}\theta\,d\Omega \tag{11}$$

The resultant domain equation still needs to be converted to the boundary, avoiding the need for domain discretization and assuring the analysis' efficiency.

As detailed in Gao (2002), the radial integration method is a purely mathematical approach to convert domain integrals into their boundary equivalents. The transformation procedure is defined by Eqs. (12) and (13).

$$\int_\Omega f(x_1, x_2)d\Omega = \int_\Gamma \frac{1}{r(q)}.\frac{\partial r}{\partial n}.F(q).d\Gamma \tag{12}$$

$$F(q) = \int f(x_1, x_2)rdr \tag{13}$$

where r is the distance between the source (p) and the collocation (q) points and n is the outward normal. Afterwards, the substitution of the obtained form of Eq. (11) into Eq. (13) results in,

$$F(q) = \int \frac{-(1+\nu)k}{2\pi(1-\nu)}r_{,i}\theta\,dr \tag{14}$$

As stated in Gao (2003), in this integration step, the derivative $r_{,i}$ is constant. This makes it possible for Eq. (14) to be written simply as,

$$F(q) = \frac{-(1+\nu)k}{2\pi(1-\nu)}\,r_{,i}\,\overline{F}(q) \tag{15}$$

for:

$$\overline{F}(q) = \int \theta \, dr \tag{16}$$

This integration step now considers only the temperature field distribution function, so, depending on the nature of the function $f(x_1,x_2)$, Eq. (16) may be analytically evaluated, increasing the computational efficiency of the method. From the resultant equations in (15) and (12), the domain integral responsible for the thermoelastic component of the deformation, obtained in Eq. (8), may now be expressed by its boundary equivalent,

$$\int_\Omega U_{ij,j} \, \tilde{k} \, \theta \, d\Omega = \int_\Gamma \frac{1}{r(q)} \frac{\partial r}{\partial n} \left(\frac{-(1+\nu)\,k}{2\,\pi\,(1-\nu)} \, r_{,i}\,\overline{F}(q) \right) d\Gamma \tag{17}$$

When substituted into Eq. (8), the equivalence of the domain and boundary integrals achieved in Eq. (17) results in the boundary exclusive integral formulation for the thermoelasticity problem,

$$\begin{aligned} c_{ij}u_j + \int_\Gamma \left(T_{ij}\,u_j - U_{ij}\,t_j \right) d\Gamma \\ = \int_\Gamma \frac{1}{r(\mathrm{q})} \frac{\partial r}{\partial n} \left(\frac{-(1+\nu)\,k}{2\,\pi\,(1-\nu)} r_{,i}\,\overline{F}(q) \right) d\Gamma \end{aligned} \tag{18}$$

Digital image correlation analysis

The DIC analysis is an optical measurement technique developed to provide displacement and deformation fields over a surface. This is achieved by comparing digital images of a surface taken before and after the application of a deformation load. This method requires the surface of interest to be marked beforehand with a random speckle pattern. The first part of the DIC analysis consists of an initial mapping of the undeformed marked surface, which will later be used as a reference for the correlation procedure. This mapping divides the actual surface into a subset of smaller regions positioned side by side, as illustrated in Fig. 2. For each individual sub-region, a physical point is created. After distortion, these points are used to calculate the displacements over the surface.

When mechanically loaded, the observed surface experiences a deformation that slightly distorts the marked speckle pattern. The DIC analysis procedure relies on identifying the position of the corresponding physical points on the deformed images, comparing the aspect of the marked speckle pattern before and after the deformation takes place. Due to the deformation load, the sub-regions may suffer from translation and have their boundaries deformed, as illustrated in Fig. 3. The resultant positioning of the speckles marked on the surface is then used to effectively identify the mapped sub-regions
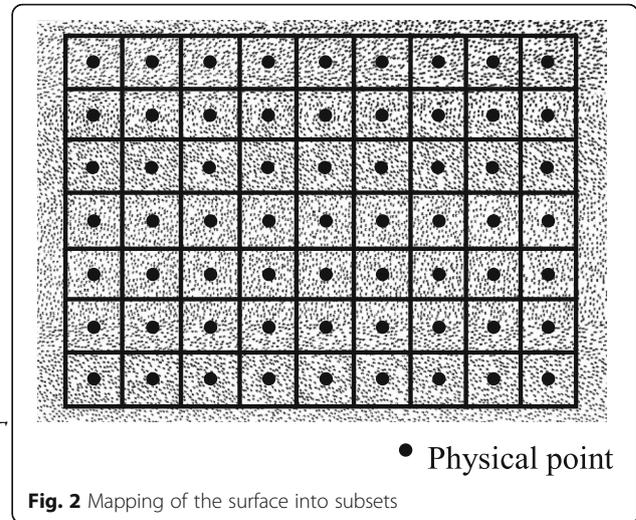

Fig. 2 Mapping of the surface into subsets

in the deformed surface image. In a monochromatic image, each pixel is associated with a discrete intensity value, $f(x,y)$, that is translated into a shade of grey. According to Pan et al. (2009), it is possible to trace the mapped subset in the deformed image from the intensity values of the pixels contained in each sub-region using cross-correlation (CC) or sum-squared difference (SSD) equations. Pan et al. (2009) also present some commonly used variations of these equations such as their normalized forms,

$$CC = \sum \left[f(x,y).g(x',y') \right] \tag{19}$$

$$SSD = \sum \left[f(x,y) - g(x',y') \right]^2 \tag{20}$$

where $f(x,y)$ and $g(x',y')$ are the intensity functions of the reference and deformed images, respectively.

As evinced in many papers, such as Pan et al. (2009), the correlation algorithm's precision relies on the size of the created sub-regions and on the quality of the speckle pattern applied to the surface. The dimensions of the mapping subsets were discussed in Pan et al. (2008) and
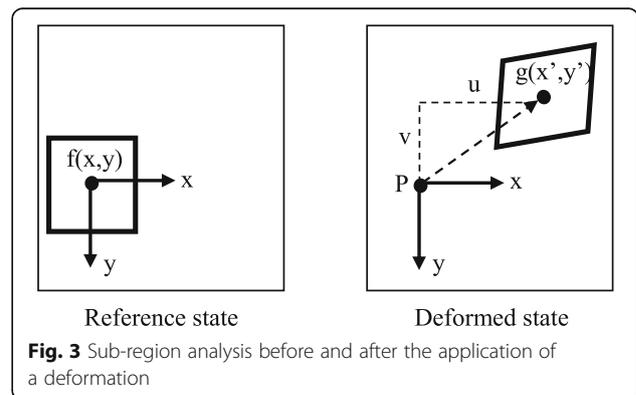

Fig. 3 Sub-region analysis before and after the application of a deformation

Sun and Pang (2007). For homogeneous materials, larger subsets tend to increase its uniqueness and, hence, decrease the correlation's random error. However, increasing the sub-region dimensions may be considered a trade-off in which the benefit for the correlation process is counterbalanced by some negative effects on other aspects of the analysis. Since there are fewer sub-regions and, hence, less physical points, the resolution of the data is reduced.

The uniqueness of the sub-regions has a close relationship with the speckle distribution pattern. Given its importance to the accuracy of correlation functions for DIC analyses, it has been the topic of interest in many recent works. By examining different speckle patterns, Pan et al. (2008) concluded that the speckle pattern applied to the surface introduces a random nature error to the analysis. Lecompte, Sol, and Vantomme (2006) numerically assessed the effects of the speckle size and their distribution density over the analysed surface. They found an optimum speckle density interval and a relationship between the sizes of the speckles and the sub-region. Later, in Lecompte et al. (2009), different sets of spray-painted speckle patterns were experimentally analysed with imposed displacement. Their results showed that patterns composed of larger speckles resulted in increased random errors while patterns composed of smaller speckles resulted in both increased random and systematic errors. Combining the information provided in these works, it is possible to numerically generate a theoretically adequate speckle pattern for DIC analysis in regard to the speckle size and distribution.

As stated in Crammond et al. (2013), many quality assessment parameters have been developed to evaluate speckle patterns. However, since it is based strictly on numerical analysis, most of these parameters end up as comparative tools. Unlike purely numerical analysis, the practical aspects of the analysis, as the application method used to create the pattern on the surface or even the DIC equipment itself, turn each problem into an almost unique condition. For this reason, Barranger et al. (2010) presented an experimental procedure to assess the influence of practical aspects of the DIC analysis on the expected results. They focused on the type of camera and speckle used in the analysis. In Crammond et al. (2013), two different random pattern creation methods were investigated, airbrush and spray painting. Their experimental results showed that more even speckle distributions (achieved by airbrushing) contributed to more accurate results. They also stated that both explored techniques provided poor control of important pattern features, such as speckle size and distribution.

To overcome these problems with spray and airbrush painting techniques, Mazzoleni et al. (2015) proposed an alternative method for transferring computer-generated random speckle patterns to surfaces for DIC analyses using a thermo-mechanical toner. This method allows good control over the generated speckle pattern, enabling analyses on various scales. Inspired by the Mazzoleni et al., an alternative speckle pattern transfer method was developed to ensure the quality of the speckle patterns used for DIC analyses in this work. The developed method consists of marking the target surface with randomly positioned dots using a CNC marker device specially designed for this purpose. The designed device is basically a mechanism capable of moving a permanent ink marker pen over the target surface and marking a circular dot when certain coordinates are reached. The movements, limited to a plane parallel to the surface to be marked, are controlled by two stepper motors, while the marking motion is performed by a servo motor. Regarding the marking process, a 1.0-mm pen was used to reproduce the speckles numerically generated in the computer over the actual surface. From previous tests, these kinds of marker pens can produce speckles with an average of 0.6 ± 0.1 mm of diameter, sufficient to fulfil the experimental scaling requirements for this work. A prototype of the designed equipment is exhibited in Fig. 4a. Applying the 40% of the surface area occupied by a speckle guideline suggested in Lecompte et al. (2006) to the computationally generated speckle pattern leads to the pattern presented in Fig. 4b.

Table 1 presents the generated speckles and their respective pattern histogram. A histogram is a graphical representation of the pixels exposed in an image. The left side of the graph represents the blacks or shadows while the right side represents the highlights or bright areas. The middle section is mid-tones and represents the amount of grey tones present between the extremes of white and black. The histogram obtained from the CNC marker and the one made by spray painting can be compared. Histogram #1 presents two peaks very well pronounced on the left and right, representing the tones nearest to black and white, while in Histogram #2, the pronounced peak shows the strong presence of white. This observation can be done when the pictures of each process used to generate the speckle pattern are observed simultaneously. The CNC marker picture presents an equal distribution between white, black and grey. The same cannot be said about the image that depicts the spray-painted speckle pattern, where significant portions of the area in white are very prominent. However, if attention is focused on the greyscale, it is possible to see that the grey distribution is much more constant for the speckle pattern generated by CNC marker than those obtained by spray marker. In addition to these observations, it must be highlighted that the CNC marker never changes the histogram while the same cannot be said about spray paint process due to

Fig. 4 a CNC marking device prototype marking a surface painted white. **b** Resultant printed speckle pattern with 40% of the total area covered with black speckles

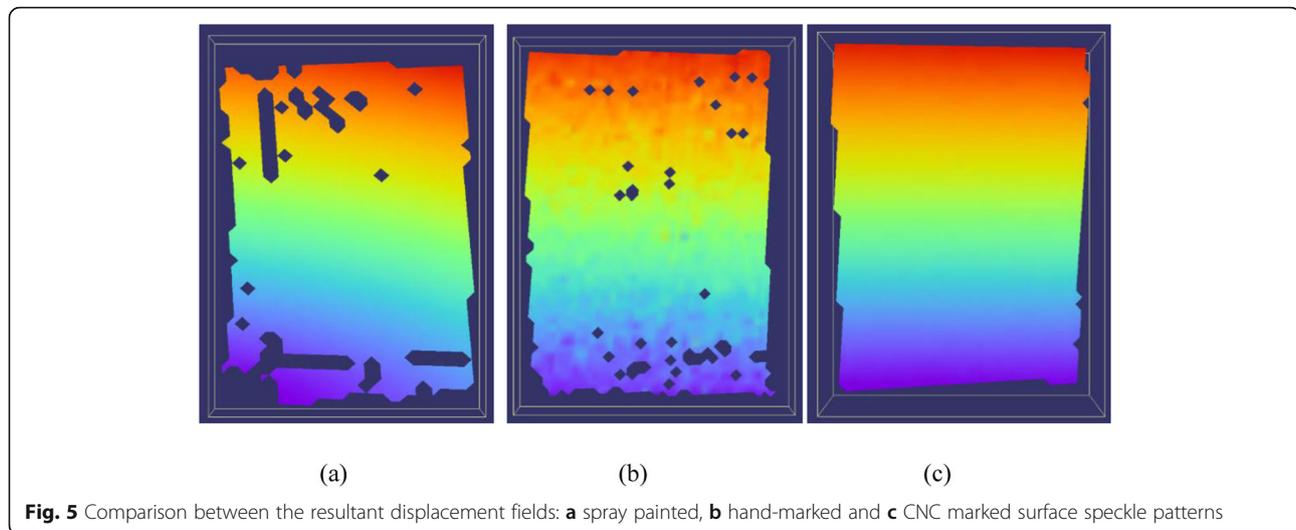the randomness of the process employed (Zhang et al., 2018).

The benefits of the developed surface marking procedure can be stated in the comparison presented in Fig. 5. Three specimens were prepared using spray paint, hand-marked points and the CNC marking device. The DIC analyses were performed using a Dantec Dynamics Q-400 DIC system and a comparison resulting from the DIC data acquisition can be seen in Fig. 5, where the continuity of the displayed fields evinces the better performance of the CNC marked pattern.

The disturbance noticed in the DIC figure corresponding to the hand-marked pattern can be ascribed to the small density of points marked and the lack of randomicity in the obtained pattern, which negatively affects the correlation step performed in the DIC analysis. Adhesives with a random speckle pattern are commercially available but they are expensive and can be used only once. Furthermore, such adhesives cannot be applied to complex surfaces or at high temperature, thus limiting the use. In the case of complex geometries, the only alternative is to prepare the component by spraying the paint manually. Generally, a high-quality speckle pattern is not reached manually, and some data are lost during the process of data acquisition. A special routine was written based on the speckle

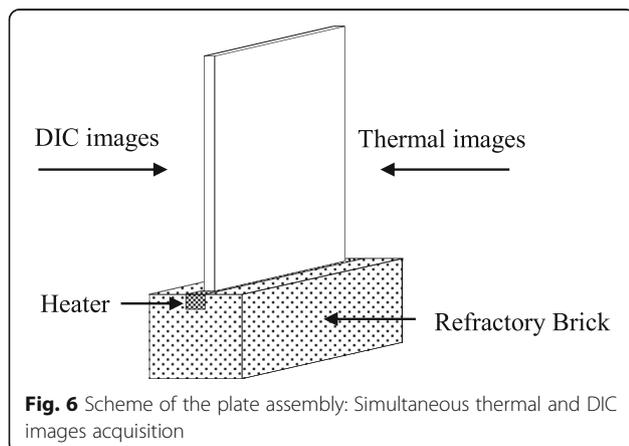**Table 1** Comparison of the processes used to generate the speckle pattern

Pattern #	Image	Histogram
#1—CNC marker		
#2—Spray painted		

Fig. 5 Comparison between the resultant displacement fields: **a** spray painted, **b** hand-marked and **c** CNC marked surface speckle patterns

pattern obtained from the commercial adhesives and reproduced by the CNC marker introduced in this work. It is important to highlight that the present methodology can be adapted for any other device, like 3d printers, to mark the speckle patterns independent of the surface complexity.

Results and discussion

Verification of the numerical BEM formulation for thermoelasticity using RIM required an experimental setup capable of providing, simultaneously, the temperature field acting over the target surface and its consequent displacement field. To fulfil this requirement, an experimental assembly was elaborated based on thermal image acquisition of the temperature fields acting over a surface and DIC to provide the resultant displacement field caused by a heating process. Similar strategies were applied in Bodelot et al. (2009) and Silva and Ravichandran (2011). Both these works focused on acquiring thermal and DIC images over the same surface. Silva and Ravichandran (2011) developed a piece of single equipment

Fig. 6 Scheme of the plate assembly: Simultaneous thermal and DIC images acquisition

capable of collecting both data types at the same time. In a different way, Bodelot et al. (2009) used a dichroic mirror, which is exclusively translucid to infrared wavelengths. While the infrared wavelengths were directly captured by the thermal camera and processed to give the acting temperature field, the remaining wavelengths were reflected to the DIC system and used to evaluate consequent displacement fields. However, as stated in these works, both DIC and thermal imaging data acquisition methods rely on surface readings with different surface preparation requirements. DIC requires the analysed surface to have a speckle pattern marked over it, while to assure the precision of the thermographic images, the surface must be prepared in a way to maximize and homogenize its infrared emittance, in accordance with Dondero et al. (2011). In furtherance of overcoming this issue, Silva and Ravichandran (2011) opted for preparing the surface to be simultaneously measured with a high-emittance base coating and applying a lower-emittance speckle pattern that covered only 10% of the surface area. In a similar way, the simultaneous analysis presented in Bodelot et al. (2009) required the development of a special coating.

To avoid the necessity for special coatings and allow a speckle pattern area coverage of around 40%, as suggested in Lecompte et al. (2006), this work proposes a different experimental setup. As in Bodelot et al. (2009), the proposed experimental setup uses two separate apparatuses for acquiring the thermal images and the DIC surface images. However, instead of having both acquiring information from the same surface, in the planned assembly, the thermal and DIC cameras are placed facing toward opposite faces of a relatively thin vertically positioned rectangular plate. Assuming uniform heating at the base of the plate, a controlled environment and only natural convection acting at the remaining edges,
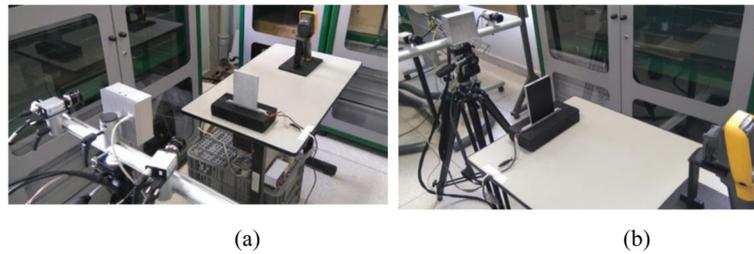
Fig. 7 Experimental assembly: **a** DIC system point of view, **b** thermal imager point of view

both opposite faces used for data acquisition experience the same temperature gradients. In this sense, both faces experience the same resultant displacement field.

The plate is mounted vertically over a heater responsible for generating a temperature gradient over the plate, as illustrated in Fig. 6. A high wattage cartridge heater was selected for this experiment due to its uniform heating characteristic. In furtherance of maximizing the heat flux to the plate and avoiding any damage to other experimental components, the heater was placed inside a groove carved in the surface of a refractory brick. Thermal paste was also applied to the contact region between the heater and the plate to ensure the desired uniform thermal conductivity.

The plate used in the experiment was manufactured from ASTM 6351 aluminium alloy with dimensions of $140 \times 102.6 \times 9.6$ mm. Since, in this setup, the DIC images and thermal images were taken on different sides of the plate, each side was prepared accordingly. The side used for the DIC analysis received a thin coat of matte white spray paint before having a speckle pattern

Fig. 8 Steady-state thermal image of the plate surface (*colour should be used in print*)

marked over it using the designed CNC marker. The applied thin white layer serves two purposes: to eliminate the reflectivity, characteristic to aluminium alloys, and increase the contrast between the speckle pattern and the surface background. The opposite side of the plate, used for the thermal images, was painted matte black, as in Dondero et al. (2011). The complete experimental assembly is shown in Fig. 7 a and b. This picture also shows the Fluke Ti 125 thermal camera, positioned facing the black painted side of the plate, while the Dantec Q-400 DIC system is positioned facing the opposite face.

The experimental procedure has two main steps: reference image acquisition and steady-state image acquisition. The first step, performed before heating, serves the purpose of acquiring the reference image for the DIC analysis, which will be used by the DIC system to calculate the resultant displacement fields at the end. At this step, an initial temperature reading of the plate is also performed. The plate should, at this point, be entirely at room temperature, θ_0. After that, the plate is slowly heated until the steady-state condition is achieved, at which point a new set of DIC and thermal images are taken.
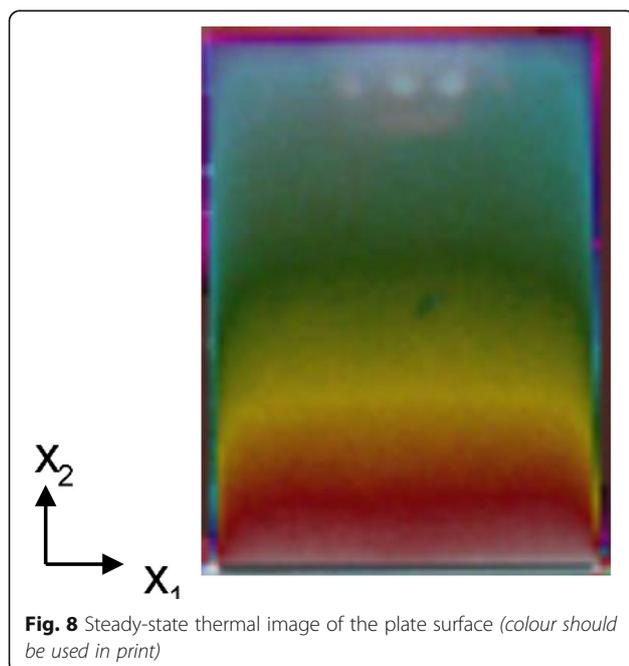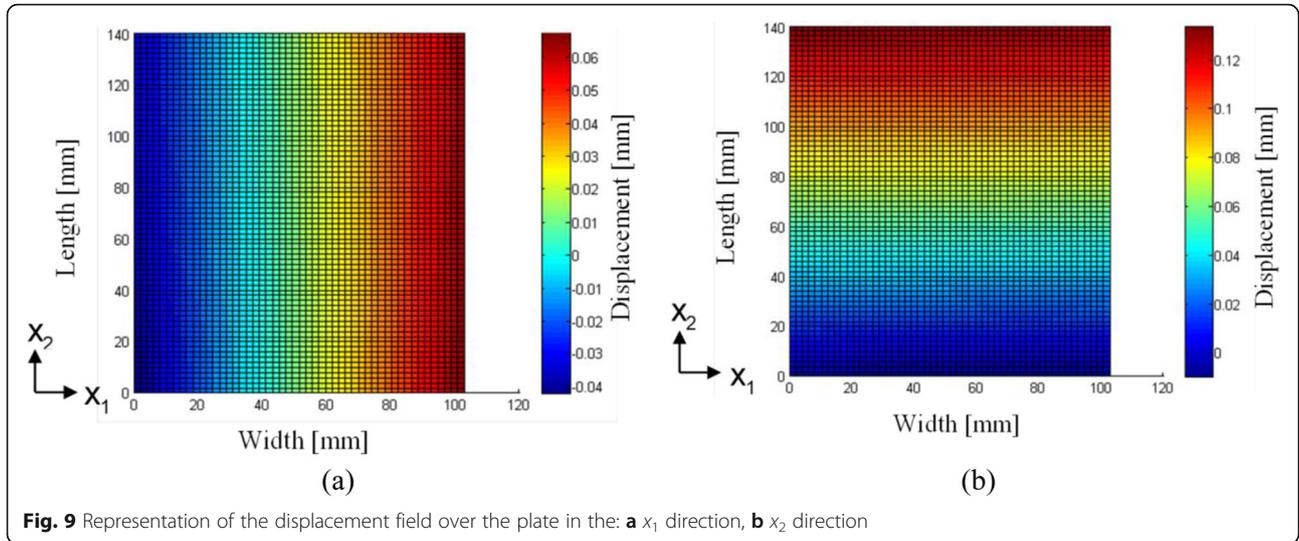
Experimental results

Figure 8 shows the steady-state thermal image obtained for the observed plate. The symmetric aspect of the isothermal curves indicates even heating over the base of the plate. At the inner regions of the plate, the registered temperature field presents a considerably linear behaviour in the x_2 direction. However, at regions closer to the surface top and lateral edges, the temperature rapidly decreases as an effect of the heat loss caused by natural convection.

The DIC results show that more than 1600 physical points were automatically generated during the mapping step. Given the relatively reduced dimensions of plate analysed, this number of physical points permitted fine analysis of the resultant displacements. It also points out the good performance of the speckle pattern generation and transfer methodologies applied for this work. Figure 9 a and b show representations of the displacement field determined by the DIC analysis over the plate in the x_1 and x_2 directions, respectively.

Fig. 9 Representation of the displacement field over the plate in the: **a** x_1 direction, **b** x_2 direction
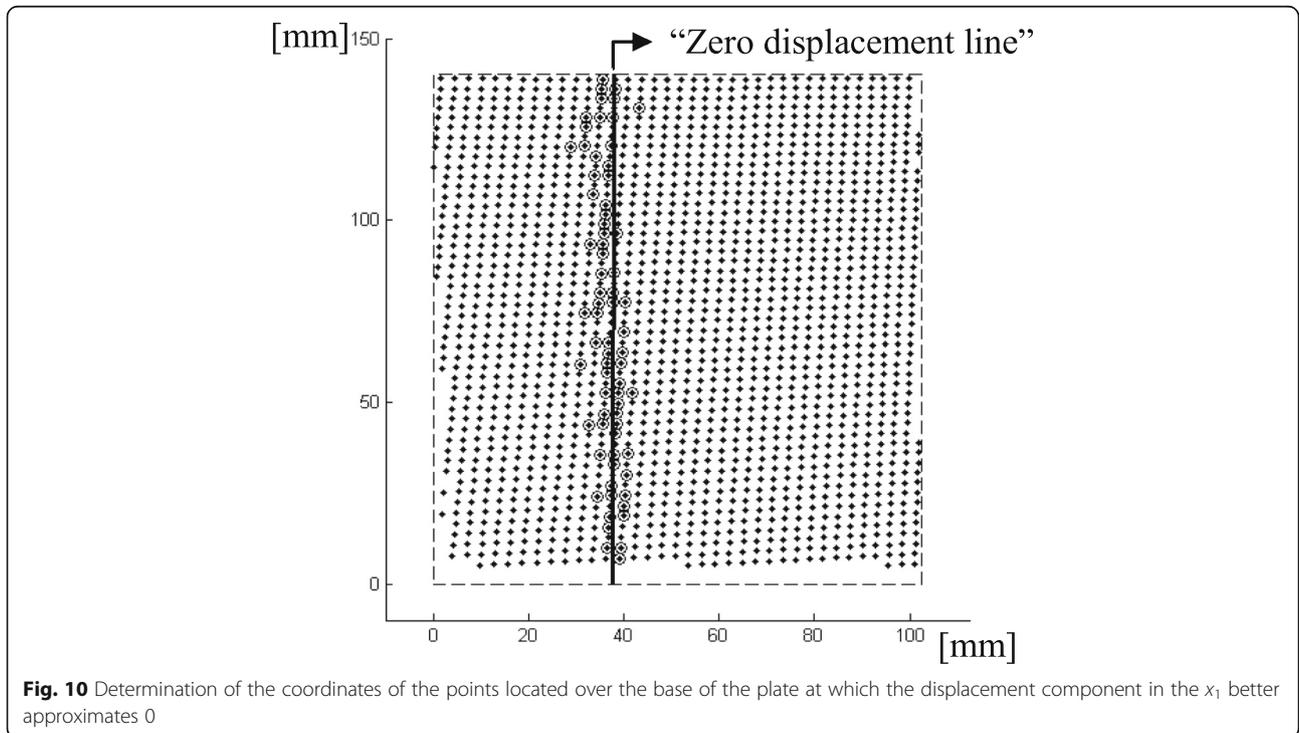
The graphical analysis of the individual displacement components, shown in Fig. 9 a and b, evinces the relatively linear behaviour of the components in both directions. In addition, from Fig. 9 a, it is noticeable that the region with null displacement in the x_1 direction is not coincident with the exact centre of the plate. In fact, the results show that this region is located approximately 40 mm from the left edge of the plate due to the thermal expansion allowed by the thermal paste applied to the contact region between the heater and the plate.
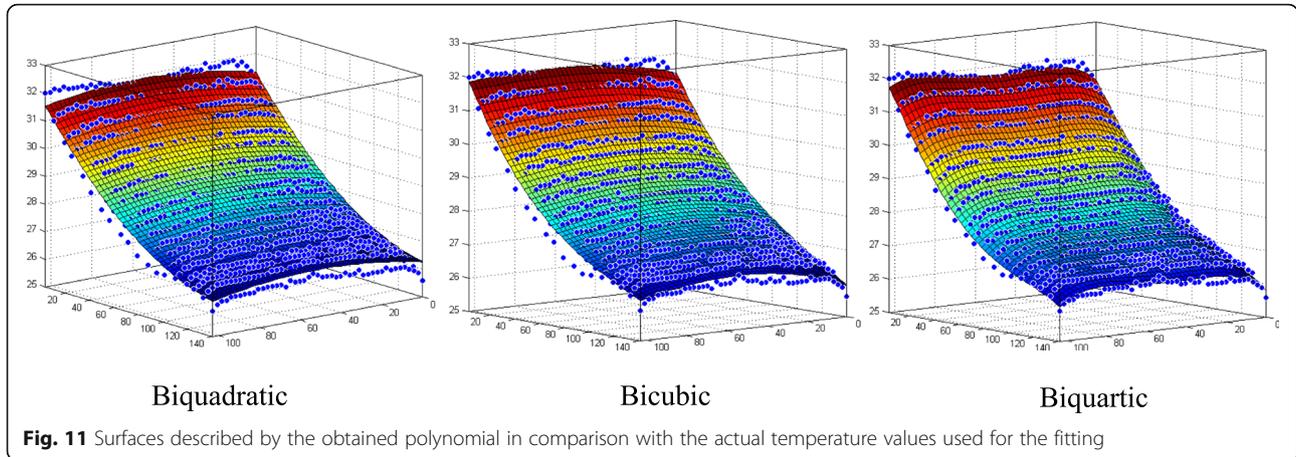
Figure 10 depicts the physical points generated during the mapping process in the DIC analyses marked as black dots

in the interior of the plate. In this figure, the circled points represent the set of physical points used in the regression that originated the "zero displacement line" at 38.1 mm.

Numerical results

The BEM formulation for thermoelasticity developed using RIM requires the boundary condition that describes the temperature field in the model to be defined by a function $\theta(x_1, x_2)$. The thermoelastic problem is solved using BEM. To determine the strain field, it is necessary to determine the temperature field inside the domain. In this thermoelastic analysis, the strain field results from the thermal expansion

Fig. 10 Determination of the coordinates of the points located over the base of the plate at which the displacement component in the x_1 better approximates 0

| Biquadratic | Bicubic | Biquartic |

Fig. 11 Surfaces described by the obtained polynomial in comparison with the actual temperature values used for the fitting

due to field temperature generated inside the domain. The field temperature is represented by an integral domain that must be converted to an equivalent boundary integral. RIM is the methodology employed to perform this equivalence, thus preserving all advantages provided by BEM. The experimental data for the steady-state temperature field can be recovered by determining $\theta_{ss}(x_1, x_2)$ from data obtained over the plate's surface via thermal images.

Considering the constant room temperature (θ_0) condition at the reference step, the temperature variation caused by heating for a set of i different punctual locations over the plate can be defined by,

$$\theta_i = \theta_{ss}(x_{1_i}, x_{2_i}) - \theta_0 \tag{21}$$

The experimental discrete temperature values data must be approximated by a polynomial function, allowing it to be analytically evaluated using Eq. (16). For the sake of completeness, three different polynomial fittings for $\theta(x_1, x_2)$ were considered, biquadratic, bicubic and

Fig. 12 Selected positioning to evaluate the numerical and experimental results
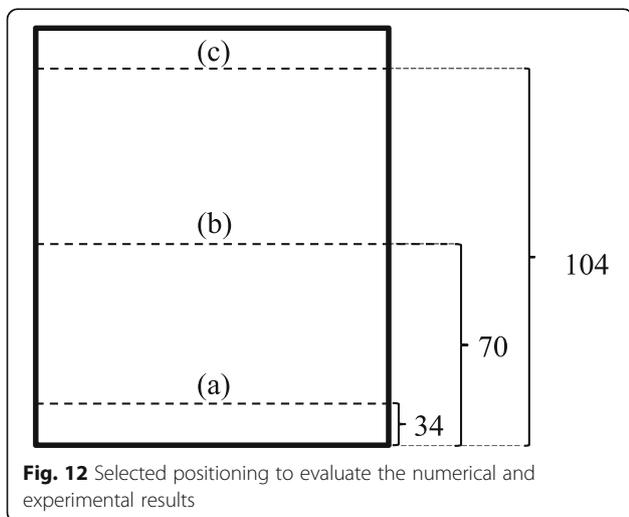
biquartic. In Fig. 11, the continuous surface represents the experimental data while the small circles represent the actual values of temperature used for the fitting.

The obtained $\theta(x, y)$ functions were then applied to the BEM formulation and the resultant numerical displacements were compared to the experimental displacement values obtained via DIC analysis. To compare the numerical and experimental displacements, three horizontal lines, positioned at 34, 70 and 104 mm over the plate, where chosen (Fig. 12). The lines' position over the plate was chosen to control the temperature field near the boundary condition region, in the middle and near the top of the plate. Due to the linear temperature distribution, with these three lines, one can easily validate the numerical and experimental procedures. Figure 13 presents the resulting comparison for each line. It is possible to observe the resultant displacements for the three types of polynomial functions (biquadratic, bicubic and biquartic) used to approximate the temperature field.

A relatively good approximation between the numerical and experimental results is already noticeable, which points out the good performance of the proposed experimental methodology. The maximum and root mean square (RMS) errors were calculated for each set of numerical results. Using the experimentally obtained results as a reference, the maximum error provides an evaluation parameter of the error over each line, while the RMS (Eq. 22) gives an average evaluation of the error considering the entire line. These two sets of errors provide sufficient information to comparatively evaluate the performance of each polynomial approach.

$$E_{rms} = \sqrt{\frac{\sum_{i=1}^{n} \left(D_i^{Exp} - D_i^{Num}\right)^2}{n}} \tag{22}$$

where D_i^{Exp} and D_i^{Num} stand for the experimentally and numerically obtained displacements, respectively. The resultant error values are presented in Tables 2 and 3.
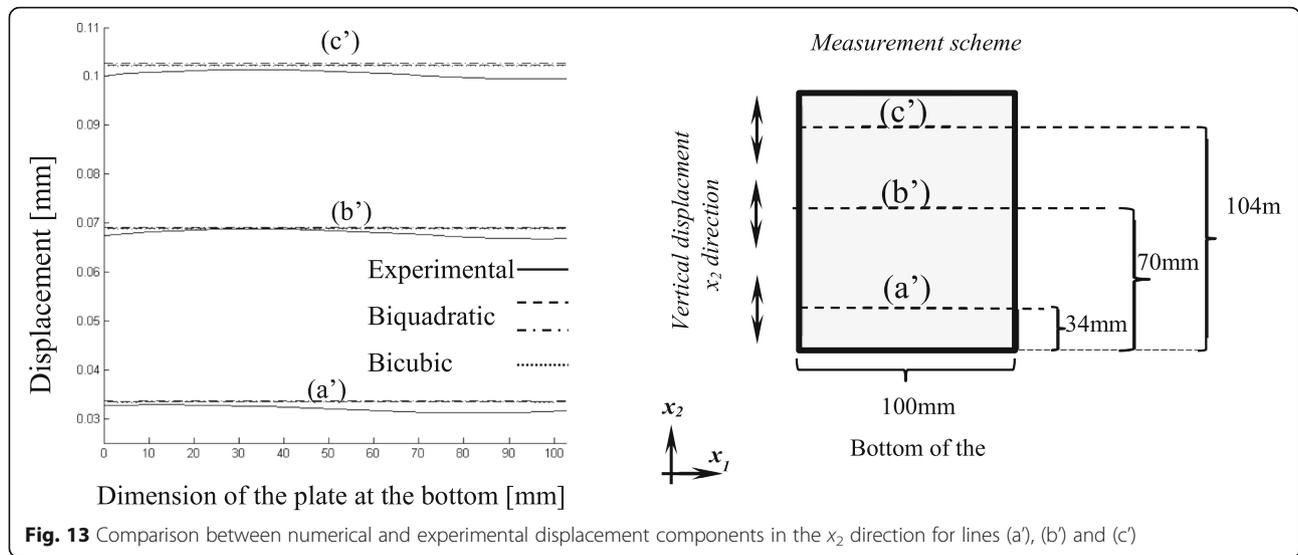
Fig. 13 Comparison between numerical and experimental displacement components in the x_2 direction for lines (a'), (b') and (c')

The proximity of the resultant values provided by each polynomial function, Fig. 13, is once again evinced by the error data contained in Tables 2 and 3. Even though a better performance of the biquartic function was expected, since it better approximated the temperature field, the error data points out a minimal difference, of order 10^{-4}. In this sense, any of the tested polynomial functions are relatively well suited for this kind of thermoelastic analysis without loss of accuracy.

The displacement in the x_2 direction for line (b') presented the lowest maximum and RMS errors. One of the reasons is that line (b') is less influenced by the surroundings of the experimental setup, such as background illumination and possible reflections. Line (c'), near the top of the plate, was more susceptible to background lighting interference. Those regions near the bottom of the plate are subjected to a different kind of interference. Even painted with considerably low reflectivity paint, the reflection caused by the diffuse environmental lighting cannot be fully avoided. These effects can be confirmed by evaluating line (a'), depicted in Fig. 13b, which corresponds to a position near the mounting area. The reflectivity issue was also reported in the DIC analysis, causing some physical points to be discarded.

Conclusions

This work presented a methodology for thermoelastic analysis using BEM and experimental temperature data based on thermal images. In this proposed methodology, the experimentally acquired temperature fields were used as inputs for a numerical BEM routine that calculates the consequent displacement fields. The BEM formulation used in this procedure, obtained from an RIM application, required the temperature field to be input as a function, introducing a possible error source to the analysis. The elaborated experimental procedure relied on the simultaneous acquisition of the temperature and displacement fields acting on a surface using two optical measurement methods, thermal imaging and DIC analysis. The good quality of the speckle pattern used in the DIC analyses was assured by using a CNC marker device specially developed for this work. Its good performance was evinced in a comparative analysis against patterns obtained from other techniques, such as spray painting, that showed considerable data loss. The present CNC marker can be adapted for generating a speckle pattern on components with complex geometries without loss of data acquisition. A comparison between the numerical (BEM) and experimental (DIC) displacement fields

Table 2 Maximum and RMS errors for each polynomial approximation for the displacement components in the x_1 direction

Line	Biquadratic		Bicubic		Biquartic	
	Max.	RMS	Max.	RMS	Max.	RMS
(a)	0.0035	0.0019	0.0033	0.0018	0.0036	0.0020
(b)	0.0022	0.0021	0.0022	0.0021	0.0024	0.0022
(c)	0.0034	0.0027	0.0036	0.0027	0.0033	0.0028

Table 3 Maximum and RMS errors for each polynomial approximation for the displacement components in the x_2 direction

Line	Biquadratic		Bicubic		Biquartic	
	Max.	RMS	Max.	RMS	Max.	RMS
(a)	0.0023	0.0016	0.0024	0.0017	0.0022	0.0015
(b)	0.0021	0.0012	0.0023	0.0014	0.0019	0.0011
(c)	0.0029	0.0019	0.0032	0.0022	0.0026	0.0017

pointed out the good accuracy of the proposed methodology. The observed good agreement between the numerical and experimental results points toward the viability and good accuracy of the proposed methodology. Finally, the present methodology covered the subject of thermoelasticity from numerical and experimental points of view and the good obtained results allow its application for more complex analysis, including nonlinearities.

Authors' contributions
The work is carried by the corresponding author CTMA. All authors read and approved the final manuscript.

Funding

Competing interests
The authors declare that they have no competing interests.

References
Aliabadi, M. H. (2002). *The boundary element method, volume 2, applications in solids and structures* (1st ed.). Chichester: Wiley.

Banerjee, P., & Butterfield, R. (1981). *Boundary elements method in engineering science*. London: Mcgraw-hill.

Barranger, Y., Doumalin, P., Dupré, J. C., & Germaneau, A. (2010). Digital image correlation accuracy: Influence of kind of speckle and recording setup. In *EPJ web of conferences volume 6 - ICEM 14 – 14th International Conference on Experimental Mechanics, Poitiers, France*.

Bodelot, L., Sabatier, L., Charkaluk, E., & Dufrénoy, P. (2009). Experimental setup for fully coupled kinematic and thermal measurements at the microstructure scale of an AISI 316L steel. *Materials Science and Engineering A, 501*, 52–60.

Brebbia, C. A., & Dominguez, J. (1996). *Boundary elements: An introductory course* (2nd ed.). Southampton: WIT Press.

Chen, D., Sun, S., Dulieu-Barton, J. M., Li, Q., & Wang, W. (2018). Crack growth analysis in welded and non-welded T-joints based on lock-in digital image correlation and thermoelastic stress analysis. *International Journal of Fatigue, 110*, 172–185.

Crammond, G., Boyd, S. W., & Dulieu-Barton, J. M. (2013). Speckle pattern assessment for digital image correlation. *Optics and Lasers in Engineering, 51*(12), 1368–1378.

Cruse TA. (1975). Boundary integral equation method for three-dimensional elastic fracture mechanics, In: AFOSR-TR-75-0813, ADA 011660, Pratt and Whitney Aircraft, Connecticut, Interim scientific rept. 1 Apr 74–31 March 1975.

Danson, D. J. (1981). A boundary element formulation for problems in linear isotropic elasticity with body forces. In C. A. Brebbia (Ed.), *Boundary element methods* (pp. 105–122). Berlin: Springer.

Dondero, A., Cisilino, A. P., Carella, J. M., & Tomba, J. P. (2011). Effective thermal conductivity of functionally graded random micro-heterogeneous materials using representative volume element and BEM. *Intenational Journal of Heat and Mass Transfer, 54*(17–18), 3874–3881.

Gao, X. W. (2002). The radial integration method for evaluation of domain integrals with boundary-only discretization. *Engineering Analysis with Boundary Elements, 26*, 905–916.

Gao, X. W. (2003). Boundary element analysis in thermoelasticity with and without internal cells. *International Journal for Numerical Methods in Engineering, 57*(7), 975–990.

Katsikadelis, J. T. (2002). *Boundary elements: Theory and applications* (1st ed.). Oxford: Elsevier.

Krishna, B. M., Tezeswi, T. P., Kumar, P. R., Gopikrishna, K., Sivakumar, M. V. N., & Shashi, M. (2019). QR code as speckle pattern for reinforced concrete beams using digital image correlation. *Structural Monitoring and Maintenance, 6*(1), 67–84.

Lecompte, D., Bossuyt, S., Cooreman, S., Sol, H., & Vantomme, J. (2009). Study and generation of optimal speckle patterns for DIC. In *Proceedings of SEM annual conference & exposition on experimental and applied mechanics, Orlando, United States*.

Lecompte, D., Smits, A., Bossuyt, S., Sol, H., Vantomme, J., Van Hemelrijck, D., & Habraken, M. A. (2006). Quality assessment of speckle patterns for digital image correlation. *Optics and Lasers in Engineering, 44*(11), 1132–1145.

Lecompte, D., Sol, H., & Vantomme, J. (2006). Analysis of speckle patterns for deformation measurements by digital image correlation. In *Proceedings of SPIE vol. 6341, Speckle06, From Grains to Flowers, Nimmes, France*.

Mazzoleni, P., Zappa, E., Matta, F., & Sutton, M. A. (2015). Thermo-mechanical toner transfer for high quality digital image correlation speckle patterns. *Optics and Lasers in Engineering, 75*, 72–80.

Nardini, D., & Brebbia, C. A. (1983). A new approach for free vibration analysis using boundary elements. *Applied Mathematical Modelling, 7*(3), 157–162.

Neves, C. A., & Brebbia, C. A. (1991). The multiple reciprocity boundary element method in elasticity: A new approach for transforming domain integral to the boundary. *International Journal for Numerical Methods in Engineering, 31*(4), 709–727.

Nowak, J. A., & Brebbia, C. A. (1989). The multiple-reciprocity method. A new approach for transforming B.E.M. domain integrals to the boundary. *Engineering Analysis with Boundary Elements, 6*(3), 164–167.

Ochiai, Y., & Kobayashi, T. (1999). Initial stress formulation for elastoplastic analysis by improved multiple-reciprocity boundary element method. *Engineering Analysis with Boundary Elements, 23*, 167–173.

Paiva, V. E. L., Gonzáles, G. L. G., Vieira, R. D., Maneschy, J. E., Vieira, R. B., & Freire, J. L. F. (2018). Fatigue monitoring of a dented piping specimen using infrared thermography. In *ASME 2018 Pressure Vessels and Piping Conference*. American Society of Mechanical Engineers Digital Collection. https://asmedigitalcollection.asme.org/PVP/proceedings-abstract/PVP2018/51586/V01AT01A034/274356. https://doi.org/10.1115/PVP2018-84597

Pan, B., Huimin, X., Wang, Z., Qian, K., & Wang, Z. (2008). Study on the subset size selection in digital image correlation for speckle patterns. *Optics Express, 16*(10), 7037–7048.

Pan, B., Qian, K., Xie, H., & Asundi, A. (2008). On errors of digital image correlation due to speckle patterns. In *Proceedings of ICEM 2008: International Conference on Experimental Mechanics, Nanjing, China*.

Pan, B., Qian, K., Xie, H., & Asundi, A. (2009). Two-dimensional digital image correlation for in-plane displacement and strain measurement: A review. *Measurement Science and Technology, 20*(6), 1–17.

Partridge, P. W., Brebbia, C. A., & Wrobel, L. C. (1992). *The dual reciprocity boundary element method* (1st ed.). Southampton: Computational Mechanics Publications.

Serrano-Munoz, I., Rapontchombo, J., Magnier, V., Brunel, F., Kossman, S., & Dufrénoy, P. (2019). Evolution in microstructure and compression behaviour of a metallic sintered friction material after braking. *Wear, 436*, 202947.

Silva, M. L., & Ravichandran, G. (2011). Combined thermoelastic stress analysis and digital image correlation with a single infrared camera. *Journal of Strain Analysis for Engineering Design, 46*(8), 783–793.

Sládek, V., & Sládek, J. (1983). Boundary integral equation in thermoelasticity. *Part I: General analysis, Applied Mathematical Modelling, 7*(4), 241–253.

Sládek, V., & Sládek, J. (1984). Boundary integral equation in thermoelasticity. *Part III: Uncoupled thermoelasticity, Applied Mathematical Modelling, 8*(6), 413–418.

Sun, Y. F., & Pang, H. J. (2007). Study of optimal subset size in digital image correlation of speckle pattern images. *Optics and Lasers in Engineering, 45*(9), 967–974.

Zhang, J., Sweedy, A., Gitzhofer, F., & Baroud, G. (2018). A novel method for repeatedly generating speckle patterns used in digital image correlation. *Optics and Lasers in Engineering, 100*, 259–266.

Publisher's Note